

# UC Berkeley

## UC Berkeley Previously Published Works

### Title

Investigation of Gold Nanoparticle Inks for Low-Temperature Lead-Free Packaging Technology

### Permalink

<https://escholarship.org/uc/item/08s2q531>

### Journal

Journal of Electronic Materials, 38(12)

### ISSN

1543-186X

### Authors

Bakhishev, Teymur  
Subramanian, Vivek

### Publication Date

2009-12-01

### DOI

10.1007/s11664-009-0918-9

Peer reviewed

# Investigation of Gold Nanoparticle Inks for Low-Temperature Lead-Free Packaging Technology

TEYMUR BAKHISHEV<sup>1,2</sup> and VIVEK SUBRAMANIAN<sup>1</sup>

1.—Department of Electrical Engineering and Computer Science, University of California, Berkeley, CA, USA. 2.—e-mail: tim\_b@eecs.berkeley.edu

Gold nanoparticle inks were investigated as a potential candidate for lead-free packaging applications. Inks consisted of surfactant-passivated nanoparticles dissolved in a solvent. Optimized gold inks are able to sinter at temperatures as low as 120°C and achieve conductivities of up to 70% of bulk. Once sintered, the metallic structure reverts to bulk-like properties and approaches bulk reliability and performance. Thus nanoparticle-based solders would operate at much lower homologous temperatures as compared with alloy-based solders. Nanoparticle inks under investigation were sintered at 180°C. The resulting material exhibited a resistivity of 5  $\mu\Omega$  cm, which is significantly lower than those of Pb-Sn and Sn-Ag-Cu. Electromigration studies were carried out and time to failure was investigated as a function of temperature. Electromigration activation energy was calculated through Black's equation to be 0.52 eV, which is consistent with surface/grain boundary diffusion. These studies suggest that nanoparticle-ink-based films show excellent robustness, due to their irreversible conversion to bulk-like materials. Nanoparticle inks are thus promising candidates for next-generation lead-free solders.

**Key words:** Lead-free, electronics packaging, low temperature, nanoparticle solder, electromigration

## INTRODUCTION

The challenges for end-of-roadmap packaging are tremendous, with steadily increasing pin count and current density requirements. Pitch requirements for high-density interconnect packages will approach 20  $\mu\text{m}$  levels, simultaneously accompanied by increases in current handling capability, particularly for analog and mixed-signal applications. These requirements place tremendous burdens on the continued viability of intermetallic eutectic solders, as these face several obstacles. First, environmental regulations have resulted in a move away from Pb-based solders. While replacement Pb-free solders have been successfully deployed in many cases, they typically offer performance characteristics that will not scale to meet end-of-roadmap requirements. Second, the use of polymer-based packages has placed constraints on the peak

processing temperatures. As the use of polymer packages increases, the need for solders that can be processed at temperatures <200°C has increased, since many low-cost polymer package materials degrade at the temperatures required for processing of conventional solders. Third, as chip densities have increased, so have pin densities. The pin densities required for package-level interconnect at the end of the roadmap are difficult to achieve using conventional solders due to poor scalability of existing solder deposition processes. Finally, as current densities rise, particularly for analog and mixed-signal parts, electromigration has become a major concern.

In this work, we investigate the properties of fused metallic inks consisting of gold nanoparticles as a potential candidate for lead-free solder. This technology achieves improvements in electrical performance and reliability in a highly scalable, polymer-substrate-compatible process. Nanoparticles are interesting candidates for solder replacements due to the remarkable physical properties

exhibited by nanosized materials. Specifically, nanoparticles have substantially depressed melting points relative to their bulk counterparts due to their enhanced surface-area-to-volume ratio.<sup>1</sup> By optimizing particle size and structure it is possible to produce films that are formed at temperatures as low as 120°C yet provide conductivities up to 70% of bulk. We have developed synthetic pathways for several metals, including Au, Ag, and Cu.<sup>2,3</sup> Nanoparticles offer several advantages over conventional solders. First, the conductivity of annealed particles is much higher than that of eutectic solders,<sup>4,5</sup> resulting in improved performance and reduced Joule-heating-induced degradation. Second, nanoparticle sintering is a one-way, irreversible process, which means that once the particles fuse the material reverts to bulk properties, including melting temperature. As a result, the formed joint has excellent thermal stability and electromigration resistance, due to significantly lower operating homologous temperature. Finally, since nanoparticles are easily dispersed into inks and printed, inkjet printing technology may be exploited to produce ultradense interconnection with <20  $\mu\text{m}$  pitch. Nanoparticle solders have been demonstrated based on silver<sup>6</sup> and tin/silver.<sup>7</sup> However, the quoted annealing temperatures of 230°C and 194°C, respectively, are noticeably greater than the temperatures achievable with our gold inks. Also, tin/silver-based solders still result in an alloy structure, with eutectic properties, as opposed to bulk properties achievable with sintered gold inks. The only other alternative capable of achieving processing temperatures as low as 120°C are solders based on tin/indium (Sn-In). However, the low melting point of the Sn-In alloy means that it would operate at a very high homologous temperature, which would significantly reduce its resistance to creep and electromigration.<sup>4,8,9</sup> Additionally, sintered nanoparticle inks offer a factor of three improvement in conductivity over Sn-In.<sup>9</sup>

## EXPERIMENTAL DETAILS

To study the viability of the metallic printed solders, optimized nanoparticles were synthesized via a chemical route developed by our group.<sup>2</sup> The inks were then printed and subjected to various annealing steps; subsequently, electrical performance, thermal annealing response, and electromigration properties were examined.

Nanoparticle inks were prepared by the Brust method as reported by Murray et al.,<sup>10</sup> where a gold precursor [hydrogen tetrachloroaurate(III) hydrate] is reduced by sodium borohydride in a two-phase reaction. Hexanethiol is used as an encapsulant which allows the particles to be dissolved in organic solvents and prevents agglomerating. The resulting nanoparticles were then extracted, washed, and redissolved in  $\alpha$ -terpineol for printing.

To measure electrical characteristics, a standard four-point test structure was utilized. Test structures

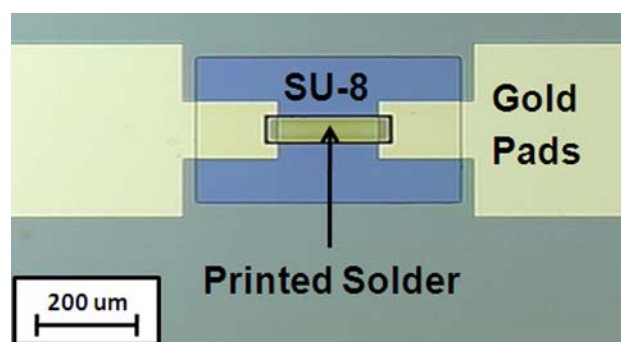


Fig. 1. Optical micrograph of a test structure.

were fabricated with a gap where the solder inks were deposited (Fig. 1). To fabricate the test structures, first gold contact pads were deposited by evaporation on top of an  $\text{SiO}_2$  substrate. Then a polymer mask was defined with SU-8 photoresist. The nanoparticle inks were then deposited in the wells using a custom-built inkjet printer. The printer used can achieve placement accuracy of 20  $\mu\text{m}$  and ink drop sizes as low as 60 pL. State-of-the-art commercial printers can achieve placement accuracies of less than 10  $\mu\text{m}$  and drop sizes of 0.1 pL. To decouple the resistance component of the ink from that of the test structure, the gap length was varied, and resistance as a function of gap length was recorded. From those data and the thickness of the deposited solder, resistivity was extracted.

Thermal annealing was performed in ambient atmosphere using a laboratory hot-plate. An oven was used for high-temperature stability testing. Electromigration tests were performed on a probe station with a temperature-controlled chuck, which allowed testing at elevated temperatures. Several samples were examined at regular time intervals during current stressing by scanning electron microscopy (SEM).

Electrical data was collected using Agilent HP4145x parameter analyzers and HP E3631A power supplies. Print line thicknesses were obtained by an Alpha-Step IQ surface profilometer. SEM was performed using a LEO 1550 scanning electron microscope.

## NANOPARTICLE INKS

Nanoparticles of a particular material generally possess many interesting properties that differ from their bulk counterparts. The property that makes nanoparticle films attractive for packaging applications is their dramatically suppressed melting temperature, which results from a high surface-area-to-volume ratio. This allows nanoparticles to bond and sinter at temperatures well below the bulk melting temperature. The size of the nanoparticles used in this study was on the order of 2 nm (Fig. 2). As synthesized, the nanoparticles are encapsulated with hexanethiol, which makes them soluble in a variety of organic solvents. Once dissolved, the

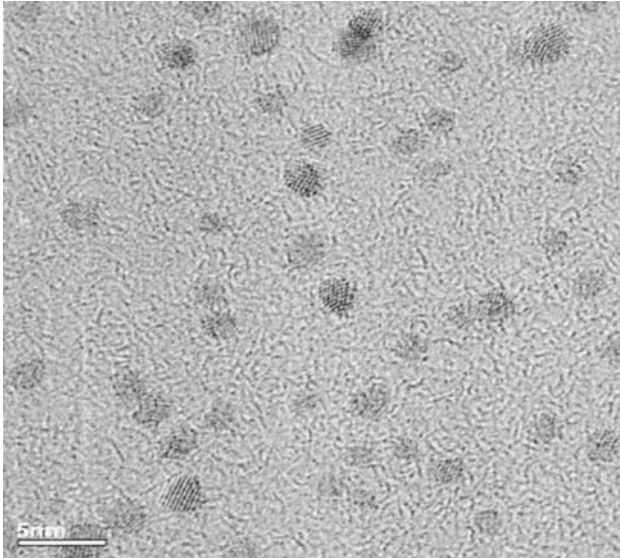


Fig. 2. Transmission electron microscopy (TEM) image of hexanethiol-encapsulated gold nanoparticles with average particle diameter of  $\sim 2$  nm.

nanoparticle-containing inks can be printed. Figure 3 shows a schematic of the sintering process. As temperature increases, the encapsulant starts dissociating from the metal and the particles start sintering together to create a continuous solid.

## RESULTS AND DISCUSSION

### Resistivity Measurement

To extract resistivity, samples with varying gap length were fabricated. The samples were annealed at  $180^{\circ}\text{C}$  for 1 h. Figure 4 shows a plot of resistance as a function of gap length for two different gap widths at a given print condition. Extrapolating those lines to zero gap length provides a value for the resistance of the evaporated test structure. Resistivity of the printed films can be calculated from the slope of the lines and the cross-sectional area of the films. Film line width is determined by the photoresist-defined print well. The thickness

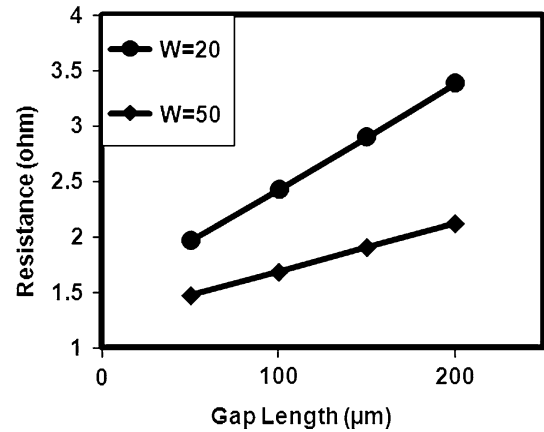


Fig. 4. Variation of resistance as a function of test structure gap length for different gap widths.

depends on various print conditions, such as print head signal voltage, print temperature, and ink viscosity.

Resistivity values were extracted to be  $5 \mu\Omega \text{ cm}$ , which is approximately twice the resistivity of bulk gold. This is significantly lower than resistivities reported for Pb-Sn, Sn-Ag-Cu, and Sn-In alloys ( $16.5 \mu\Omega \text{ cm}$ ,  $12 \mu\Omega \text{ cm}$ , and  $14.7 \mu\Omega \text{ cm}$ , respectively).<sup>4,5,9</sup> This makes nanoparticle inks better suited for highly scaled pin designs with very small pin cross-sections and high current densities.

### Thermal Properties

The effect of annealing temperature on resistance was investigated (Fig. 5). The samples were annealed for 1 h at various temperatures. It can be seen that the nanoparticle structures are conductive at  $120^{\circ}\text{C}$ , which is a significant improvement over the reflow temperatures necessary for Sn-Ag-Cu and Pb-Sn eutectic solders. It is comparable to the melting temperature of Sn-In; however, nanoparticle fused structures should offer a significant improvement in creep and electromigration stability due to a much lower operating homologous temperature. Resistance drops sharply from  $120^{\circ}\text{C}$  to

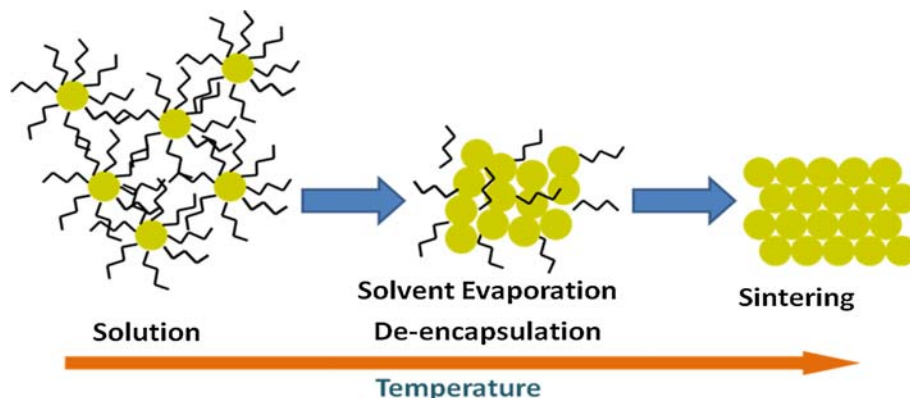


Fig. 3. Schematic of the sintering process. As temperature increases, encapsulant starts dissociating and the nanoparticles start melting. At some critical temperature the encapsulant is mostly removed and the particles sinter into a continuous film.

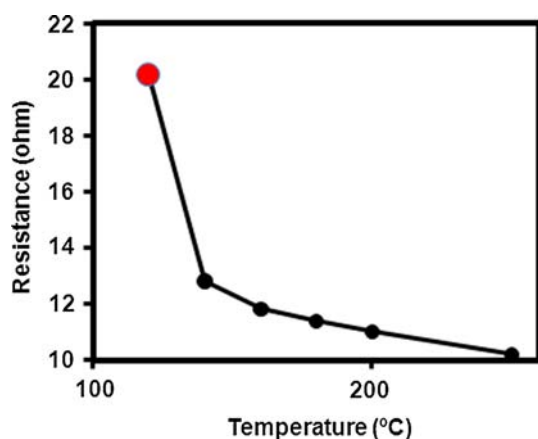


Fig. 5. Resistance as a function of anneal temperature.

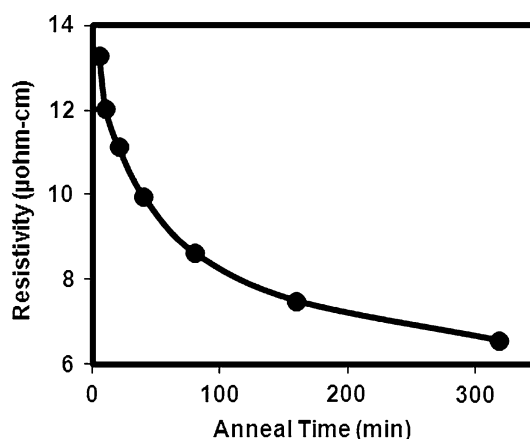


Fig. 6. Resistivity as a function of anneal time.

140°C and then asymptotes to its final value with higher-temperature anneals. Samples annealed at 300°C exhibit conductivities of  $2.7 \mu\Omega \text{ cm}$ , which approaches that of bulk gold. The melting points of various Sn-Ag-Cu alloys are on the order of 215°C to 220°C, which means that the reflow temperatures required could be as high as 250°C. Our nanoparticle inks could therefore offer operating temperature improvement of up to 130°C. Several samples were subjected to 500°C treatment and showed no signs of electrical or visible deterioration, attesting to the good thermal stability of the material. This is important, since it also suggests an overall improvement in the long-term thermal stability of these nanoparticle solder systems, compared with their eutectic solder counterparts.

The effect of anneal time on resistivity is shown in Fig. 6. Samples were annealed at 180°C for various time periods. It can be seen that the material is conductive even after 5 min of annealing. Resistivity decreases logarithmically with time. This could be explained by continuous outdiffusion of residual particle encapsulant. Low processing temperatures and fast anneal times make nanoparticle-based solders more compatible with polymer packaging, as it ameliorates the problems associated with high-temperature package degradation, thermal mismatch warping, and moisture accumulation issues.

### Electromigration

To enable rapid characterization of electromigration, initial thin test structures were fabricated. Thin samples were needed since initial tests showed that, due to the excellent robustness of these materials, very high current densities were required to induce electromigration-related failures in reasonable timescales. The starting current densities for these samples were approximately  $10^7 \text{ A/cm}^2$ . The disadvantage of using such thin samples from an experimental perspective is that the thickness ranges are at the limits of control achievable using the aforementioned printer and inkjet heads, and therefore variation in sample-to-sample thickness

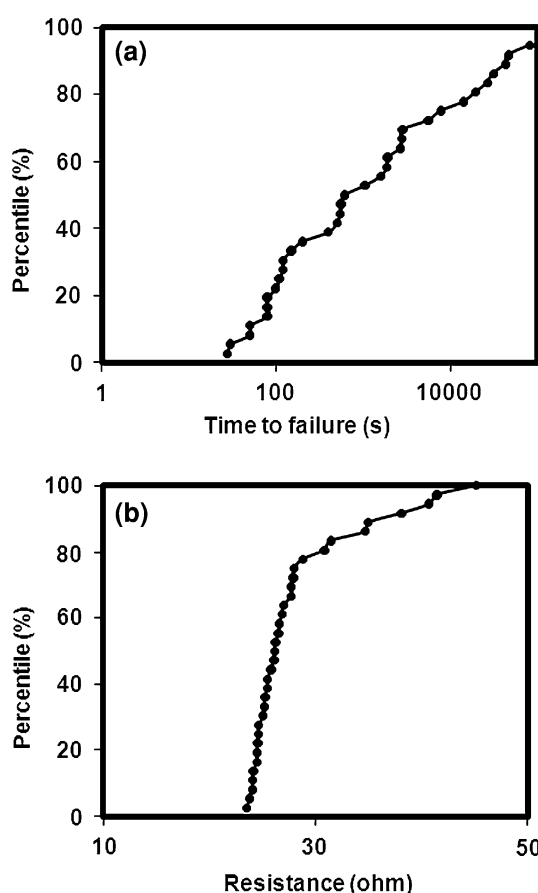


Fig. 7. Cumulative distribution for (a) time to failure and (b) resistance of thin test samples.

can be substantial. The samples were tested at room temperature. Figure 7a shows the time-to-failure distribution for the thin samples. There is a large scatter in the data, which can be attributed to variation in the thickness of the thin samples. Figure 7b shows the distribution of initial resistance of thin samples, where a significant tail can be seen. Thicker samples were fabricated in an attempt to tighten the distributions. Figure 8 shows the

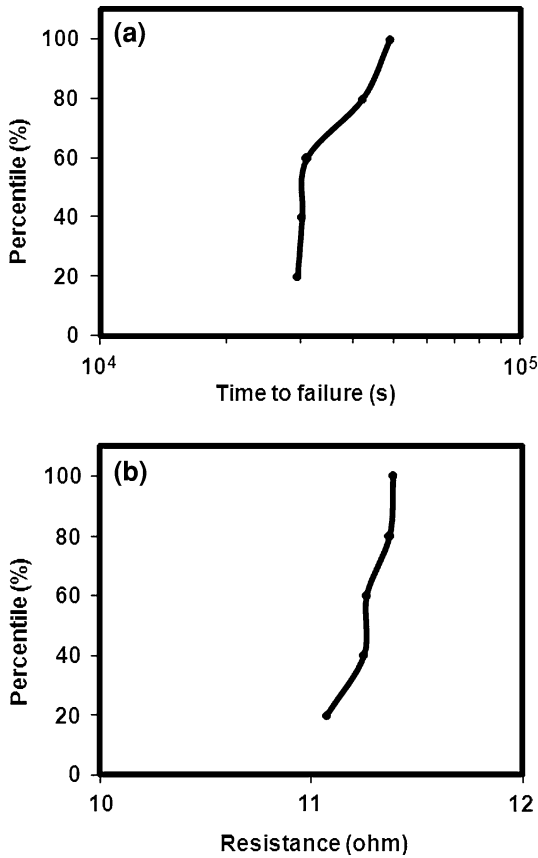


Fig. 8. Cumulative distribution for (a) time to failure and (b) resistance of thick test samples.

distributions for time to failure and initial resistance. It can be seen that the scatter is reduced significantly. The starting current density for thick samples was approximately  $10^6$  A/cm<sup>2</sup>. These samples

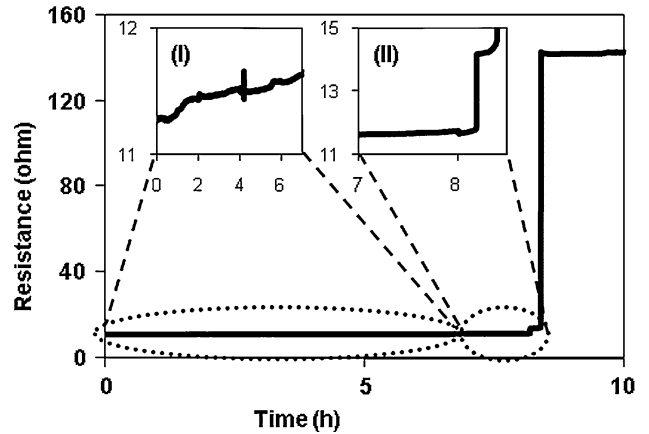


Fig. 9. Resistance as a function of stress time.

had to be tested at elevated temperatures (170°C), as they showed no signs of deterioration after a week of current stressing at room temperature.

A proposed failure mechanism was investigated. Figure 9 shows a plot of resistance as a function of stress time. Figure 10a shows a top-view SEM micrograph of a sample before and after current stressing. It can be seen that this particular sample is thicker on the sides than in the middle, which is explained by differential wetting by the ink of corners and flat surfaces. As expected most of the electron flow will proceed through the thicker parts. Insert I in Fig. 9 shows resistance for the first 7 h, which slowly increases as voids grow in the thick parts. Figure 10b shows region 1 of the sample at 2-h intervals. Steady void growth can be seen. At 8.2 h, resistance increases sharply (Fig. 9II), which suggests that there is no longer direct contact between the pads and the thicker regions. At this

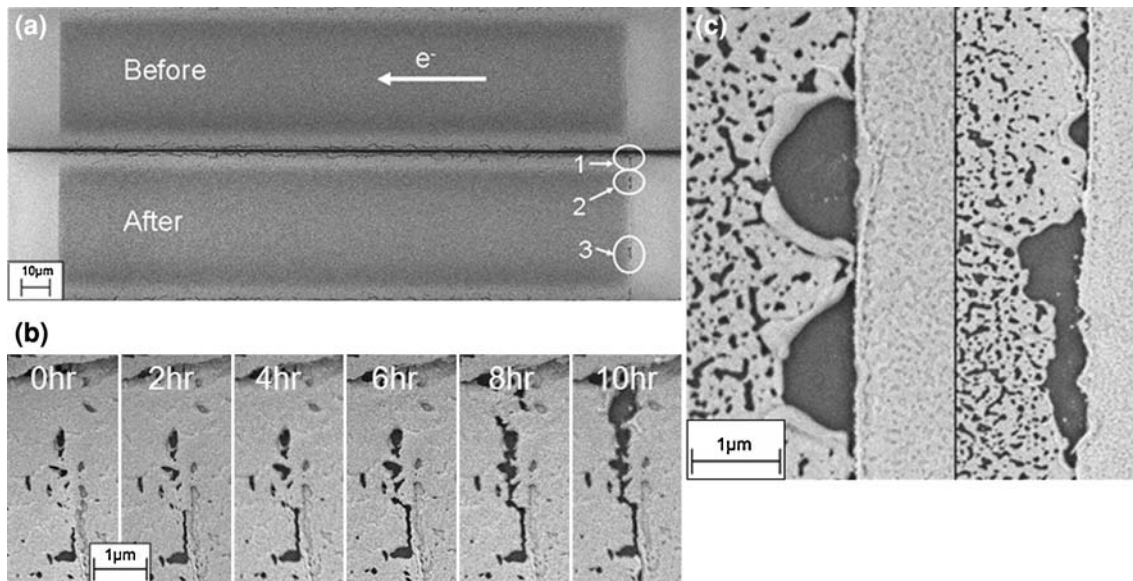


Fig. 10. SEM micrographs of a sample subjected to current stress. (a) Before (top) and after (bottom) current stress failure, (b) region 1, showing void growth at 2-h intervals, and (c) failure in regions 2 and 3.

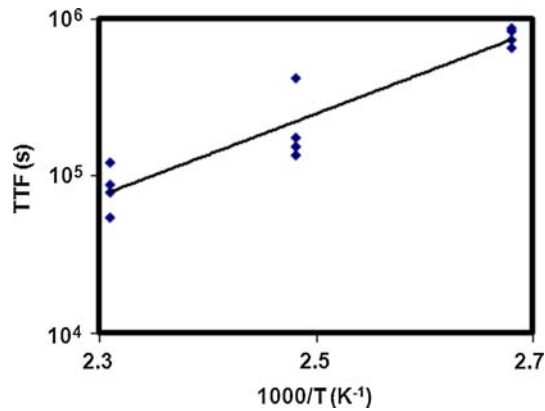


Fig. 11. Time to failure as a function of inverse temperature.

point conduction proceeds through the thinner middle of the sample and the effective current density increases dramatically. Within 12 min Joule heating destroys the remaining contact. Figure 10c shows regions 2 and 3 of the sample. Void appearance is consistent with Joule heating failure.

Several samples were driven to failure at various temperatures, and the electromigration activation energy was extracted using Black's equation<sup>11</sup>:

$$\text{MTTF} = A(J^{-n})e^{E_A/kT}$$

where  $A$  is a constant specific to the test sample,  $J$  is the current density,  $n$  is a fitting exponent (usually 1 to 2),  $E_A$  is the activation energy, and  $kT$  has its usual meaning. Figure 11 shows time to failure as a function of inverse temperature. From the line fit the electromigration activation energy for the printed ink samples is extracted to be 0.52 eV, which is in agreement with reported surface/interface diffusion numbers for gold films.<sup>12,13</sup> This is expected, as the films formed by sintering of nanoparticles are likely to be nanocrystalline.

## CONCLUSIONS

Properties of gold nanoparticle inks were examined. The nanoparticles were synthesized to form a printable ink and investigated as an option for lead-free solder applications. After heat treatment, nanoparticles would sinter into a continuous solid and revert to bulk properties. Resulting materials

are conductive after heat treatment at temperatures as low as 120°C. Sintered films exhibit resistivities up to three times lower than those of conventional eutectic alloy solders. Electromigration and thermal stability of the films were also examined and shown to be very good. Compatibility with printing techniques makes nanoparticle ink technology easily scalable to meet growing pin density demands.

## ACKNOWLEDGEMENTS

Portions of this work were supported by the National Science Foundation. Mr. Bakhishev is partially supported by an Intel Robert N. Noyce Fellowship in Microelectronics

## OPEN ACCESS

This article is distributed under the terms of the Creative Commons Attribution Noncommercial License which permits any noncommercial use, distribution, and reproduction in any medium, provided the original author(s) and source are credited.

## REFERENCES

1. P. Buffat and J.P. Borel, *Phys. Rev. A* 13, 2287 (1976).
2. D. Huang, F. Liao, S. Molessa, D. Redinger, and V. Subramanian, *J. Electrochem. Soc.* 150, G412 (2003).
3. S.K. Volkman, Y. Pei, D. Redinger, S. Yin, and V. Subramanian, *Mater. Res. Soc. Symp. Proc.* 814, 17.8.1 (2004).
4. J. Glazer, *J. Electron. Mater.* 23, 693 (1994).
5. B. Cook, I. Anderson, J. Harringa, and R. Terpstra, *J. Electron. Mater.* 31, 1190 (2002).
6. S. Joo and D.F. Baldwin, *Proceedings of Electronic Components and Technology* (2007), p. 219.
7. H. Jiang, K.S. Moon, F. Hua, and C.P. Wong, *International Symposium on Advanced Packaging Materials: Processes, Properties, and Interfaces* (2007), p. 321.
8. J. Lau and W. Dauksher, *Proceedings of Electronic Components and Technology* (2006), p. 9.
9. M. Abtew and G. Selvaduray, *Mater. Sci. Eng. Rep.* 27, 95 (2000).
10. M.J. Hostetler, J.E. Wingate, C.J. Zhong, J.E. Harris, R.W. Vachet, M.R. Clark, J.D. Londono, S.J. Green, J.J. Stokes, G.D. Wignall, G.L. Glish, M.D. Porter, N.D. Evans, and R.W. Murray, *Langmuir* 14, 17 (1998).
11. J.R. Black, *IEEE Trans. Electron. Dev.* 16, 338 (1969).
12. S. Kilgore, C. Gaw, H. Henry, D. Hill, and D. Schroder, *Mater. Res. Soc. Symp. Proc.* 863, B8.30.1 (2005).
13. M. Aguilar, A.I. Oliva, P. Quintana, and J.L. Peña, *Thin Solid Films* 317, 189 (1998).